An Interpretation on Incommensurate Structures of L-Ta$_2$O$_5$-Type Phases in the Ta$_2$O$_5$–WO$_3$ System

Toshio Miyano

Department of Science, Maizuru College of Technology, Maizuru City 625, Japan

High resolution electron microscopic (HREM) observations have revealed the existence of structures with subunits of $6.5b'$ and $8b'$ in incommensurate L-Ta$_2$O$_5$-type phases in the Ta$_2$O$_5$–WO$_3$ system, where b' is a lattice parameter of an orthorhombic β-Ta$_2$O$_5$-type subcell. Mean multiplicities $\overline{m}$ of samples annealed at several temperatures in air and Ar atmosphere were determined by means of HREM images, electron diffraction, and X-ray diffraction. Iso-mean-multiplicity lines have been proposed in the phase diagram. The lower end of a mean multiplicity of L-Ta$_2$O$_5$-type phases in the present study was about 7.0 at more than about 22 mol% of WO$_3$ content. The Ta$_{22}$W$_4$O$_{67}$ crystal, which is expected to have a mean multiplicity of 6.5, was not found. The Ta$_2$WO$_8$ crystals appeared at more than 22 mol% of WO$_3$ content. Profiles of electron diffraction intensities have been simulated based on an infinitely adaptive structure model with a solid solution, combining with data of atomic positions obtained by HREM images, which reflected a feature of experimental diffraction patterns well. © 1996 Academic Press, Inc.

1. INTRODUCTION

The phase diagram of the Ta$_2$O$_5$–Ta$_{22}$W$_4$O$_{67}$ (11Ta$_2$O$_5$4WO$_3$) system was studied by Roth *et al.* (1). Structural analyses of single crystals by X-ray diffraction were performed on the compounds Ta$_{22}$W$_4$O$_{67}$(2), Ta$_{30}$W$_2$O$_{81}$ (3), Ta$_{38}$WO$_{98}$ (4), and Ta$_2$O$_5$ (5) in this system. The intense X-ray diffraction lines could be indexed on the basis of an orthorhombic β-Ta$_2$O$_5$-type subcell with $a' \approx 6.20$ Å, $b' \approx 3.66$ Å, and $c' \approx 3.89$ Å (6). The numerous weak lines were explained by superstructures having a b axis with a *multiplicity m* of b'. Their structures were determined to have a multiplicity of 13, 8, 19, and 11. At intermediate compositions, an infinite number of compounds with ordered sequences of these modifications existed and they showed an incommensurate diffraction pattern. The incommensurate phases and the four kinds of compounds previously reported have been called L-Ta$_2$O$_5$-type structure. To explain these structures, an ideal struc-

ture model was proposed (7). The components of the superstructures are subunits with a multiplicity $m_i = 5, 8, 11, \ldots, (3i + 2)$. The superstructures are made up of the combination of adjacent two subunits. The multiplicity of the superstructure is expressed as $m = pm_i + qm_{i+1}$; here m_i and m_{i+1} are the multiplicity of adjacent two subunits and p and q are the number of the two subunits, respectively. Such superstructures are called *infinitely adaptive structures* (8, 9).

Recently, some new interpretations for incommensurate diffraction patterns of L-Ta$_2$O$_5$-type structures have been published. Schmid *et al.* described an incommensurate structure in the $(1 - x)$Ta$_2$O$_5\ x$WO$_3$ ($0 \leq x \leq 0.267$) system in terms of a *composition-dependent primary modulation wave vector* (10). They also examined the four kinds of structures previously determined by means of *apparent valence calculations*. Furthermore, Schmid *et al.* refined structures of Ta$_{22}$W$_4$O$_{67}$ and Ta$_{74}$W$_6$O$_{203}$, which have a 13 times and an 8 times superstructure, using synchrotron radiation (11). They estimated occupancies of the W atom on metal sites and vacancies of oxygen. Rae *et al.* parameterized two structures, Ta$_{22}$W$_4$O$_{67}$ and Ta$_{74}$W$_6$O$_{203}$, as composite modulated structures (12). They showed atomic modulation functions describing a structural deviation. Williams *et al.* proposed a *diagnostic parameter L* and an *approximate multiplicity* in a (001) diffraction plane of various ternary L-Ta$_2$O$_5$-related phases including the Ta$_2$O$_5$–WO$_3$ system. They found a continuum of structures explained by an *intergrowth model* using structural units with a multiplicity of 13, 16, 19, $\ldots$, 31, 34 (13). They also proposed that high resolution electron microscopic (HREM) observations described the structure of an L-Ta$_2$O$_5$-type phase in the system Ta$_2$O$_5$–TiO$_2$ as an *ordered intergrowth* of α-U$_3$O$_8$-type structure and β-U$_3$O$_8$-type structure (14, 15). Furthermore, they characterized the superstructures in terms of *shift-lattice* parameters obtained from electron diffraction patterns. A Fourier transform and an optical diffraction explained that the shift-lattice model showed incommensurate diffraction patterns (16, 17).

In a previous paper, Kosuge and I reported a contrast modulation of lattice fringes along the *b* axis in (001) images of a crystal fragment in the $Ta_2O_5-WO_3$ system by means of HREM observations (18). The contrast modulation has particular lengths of 24, 29, 35, and 40 Å, which correspond to 6.5, 8, 9.5, and 11 times *b'*, respectively. Furthermore, we have investigated sequences of the contrast modulations in observed areas and have interpreted a structural change with WO_3 content as a change of the sequence of the contrast modulation from the view point of infinitely adaptive structures. The *mean multiplicity* $\overline{m}$, which is a ratio of a mean length of the contrast modulations *S* to *b'*, has been also proposed. The value of $\overline{m}$ continuously varied with composition. England and Tilley also observed dark bands in lattice images at low magnifications (19). Papiernik *et al.* obtained an apparent multiplicity of the superstructures in the $Ta_2O_5-WO_3$ system and the ZrO_2-ZrF_4 system by electron diffraction patterns (20). The apparent multiplicity is identical to the mean multiplicity in our description. They also estimated multiplicities of the superstructures.

The present paper describes the interpretation of the relation between the superstructure and the mean multiplicity obtained from the (001) electron diffraction pattern. The incommensurate diffraction patterns have been simulated based on the infinitely adaptive structure model with a solid solution, and combined with data of atomic positions obtained by HREM observations. The mean multiplicity $\overline{m}$ of *L*-Ta_2O_5-type phases in the $Ta_2O_5-WO_3$ system depends on composition and temperature. The value of $\overline{m}$ becomes small at a higher temperature and at a higher content of WO_3. The phase diagram reported by Roth *et al.* remains unsatisfactory in the continuous change of the multiplicity with composition and temperature. The $Ta_2O_5-WO_3$ system has been reinvestigated in terms of the mean multiplicity.

2. EXPERIMENTAL

Samples used in the present study were prepared by the following method. Various proportions of Ta_2O_5 and WO_3 powder were mixed in an agate mortar and pressed into rods with a 10-mm diameter. The rods were placed into vacuum-sealed quartz tubes and heated from room temperature up to 1000°C in 5 days and held at 1000°C for 28 days. During this heat treatment the samples were ground several times so that the chemical reaction was completed. After this preliminary calcination the samples were again ground and given various heat treatments in sealed platinum tubes as shown in Table 1. Thermogravimetric analyses (TGA) in oxygen at 1000°C were also done on the samples heated in Ar.

Peak positions and intensities of the X-ray diffraction patterns of the samples were measured by a Rigaku powder diffractometer using $CuK\alpha$ radiation. A small amount of the samples were crushed in an agate mortar and dispersed in normal-butanol. A few drops of this suspension were placed on a carbon-coated holey plastic film supported by a copper grid. The crystal fragments collected on the grid were then examined by a Jeol 100CX electron microscope, operated at 100 kV, equipped with a side entry goniometer stage capable of ±25° double-tilt. HREM observations were carried out by using a Jeol 200CX electron microscope with a point-resolving power of 2.4 Å, operated at 200 kV, equipped with a top entry goniometer stage capable of ±10° double-tilt. Crystal fragments were oriented so that the [001] zone axis was parallel to the incident electron beam. The HREM images were recorded at a direct magnification of ×200,000.

Profiles of electron diffraction patterns were calculated, based on the infinitely adaptive structure model using data of atomic positions obtained from HREM images, by the FACOM computer system at Data Processing Center, Kyoto University.

3. RESULTS

3.1. HREM Observation

Figure 1 shows a HREM image down [001] of a crystal fragment of sample W12A, which contains 12 mol% of WO_3 and has been produced by heat treatment (A), taken with a 200CX electron microscope. Lattice fringes are observed with a contrast modulation along the *b* axis. The contrast modulation appears as a bright band and a dark band parallel to the *a* axis. The contrast modulation is remarkable in the inside of the crystal fragment and it is not clear at the thinner crystal edge. The minute examination on the enlarged photograph of Fig. 1 revealed that the contrast modulation is generated by a shift and growth of a black dot giving rise to lattice fringes. The examination was carried out by the following procedure:

(i) Drawing straight lines through black dots along the *a* axis at alternate dots along the *b* axis from the crystal edge to the inside area in a photograph 14 millions times enlarged;

(ii) Measuring spaces between the lines by calipers;

(iii) Measured values of spaces were classified into four levels of 5.40–5.30, 5.25–5.15, 5.15–5.05, and 4.95–4.85 mm on the photograph, which correspond to real spaces of 3.86–3.79, 3.75–3.68, 3.68–3.61, and 3.54–3.46 Å.

The variation of the space of black dots is most drastic in the dark bands. Black dots grow large with a crystal thickness. Therefore, black dots touch at narrow spaces and white dots are noticeable at wide spaces in the inside of the crystal, so that three lines of white dots in the dark bands are remarkable. The lines of white dots were used

TABLE 1
Heat Treatments of the Present Study

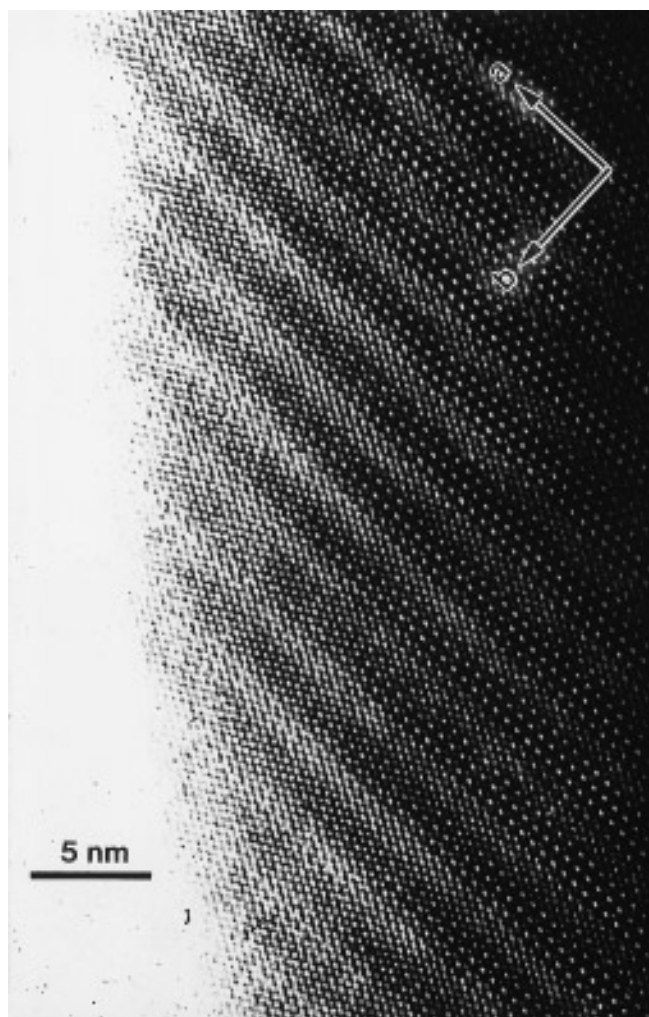| Heat treatment	Beginning temp. (°C)	Cooling rate (°C/h)	Final temp. (°C)	Annealing time (days)	Reannealing temp. (°C)	Reannealing time (days)	Atmosphere
A	1400	—	1400	14	—	—	air
B	1400	—	1400	1	—	—	air
B′	1400	—	1400	1	—	—	Ar
C	1400	—	1400	1	1000	7	air
C′	1400	—	1400	1	1000	7	Ar
D	1400	—	1400	1	700	8	air
E	1400	1.43	1200	7	—	—	air
F	1400	1.43	1000	7	—	—	air
F′	1400	1.43	1000	7	—	—	Ar
G	1400	1.43	100	—	—	—	air

FIG. 1. A HREM image down [001] of an L-Ta_2O_5-type crystal fragment of sample W12A taken with a 200CX electron microscope. Lattice fringes are observed with a contrast modulation. Dark bands appear parallel to the a axis.

as a mark to determine boundaries of subunits as mentioned below.

The image has been recorded at an optimum defocus condition in the thin region at the crystal edge, so the black dots giving rise to lattice fringes correspond to columns of metal atoms along [001] as shown in Fig. 2 which is an enlarged photograph of Fig. 1. Approximate positions of the metal atoms were determined by tracing the black dots directly onto graph paper and labeled by full circles. The black dots form a C-centered lattice, shown by a rectangle with a' and b' in Fig. 2, which is an orthorhombic subcell. The length of a subunit and the sequence of subunits were determined by the variation of the space of black dots as mentioned above. Full circles were arranged with a shift at boundaries so as to represent a dimension of a subunit. Figures by the full circles arranged denote a multiplicity of the subunit. Figure 3 shows a variation of the space along the b axis from the dot labeled by the arrow in Fig. 2. It was determined by obtained data from the enlarged photograph taking account of plane groups pm and Cm reported by Stephenson and Roth (2, 3). The space periodically varies between about 3.5 and about 3.9 Å. Waves of the variation, which correspond to subunits composing a superstructure, have lengths of $6.5b'$ and $8b'$. There is a difference between the forms of the waves with $8b'$ on both sides of the wave with $6.5b'$. This means that the b' axis of the subcell shifts by $a'/2$ at the boundary between the subunits of $6.5b'$ and $8b'$. Structure models of subunits were proposed from these data, and then intensities of electron diffraction on the models were simulated as mentioned in Section 3.5.

The contrast modulation appears in a sequence of 8, 8, 8, 6.5, 8, 8, and $8b'$ along the b axis in Fig. 2. The mean multiplicity $\overline{m}$ of this crystal fragment is 7.7, which was determined by S/b'; here S is a mean length of the contrast modulations in the whole HREM image. The value $\overline{m}$ obtained by the HREM image has uncertainness because

the observed region is limited. Electron and X-ray diffraction will give a more accurate value of $\bar{m}$.

3.2. Electron Diffraction

A (001) electron diffraction pattern of an L-Ta$_2$O$_5$-type crystal consists of fundamental spots indexed by the orthorhombic subcell and superstructure spots, as shown in Fig. 4. The diffraction spot indexed as (110) has a very strong intensity in X-ray diffraction. The next spot on the right side of the (110) spot corresponds to a C-line characterized by powder X-ray diffraction (21). The spacings and the positions of the superstructure spots are sensitive to WO$_3$ content. Figure 5 shows arrays of (1k0) electron diffraction spots of each sample annealed at 1400°C in air, where k denotes an index by a superlattice. The spots indicated by

FIG. 3. A variation of the spacing between the black dots along the b axis from the dot labeled by the arrow in Fig. 2. A period of the variation corresponds to a subunit. A wave form of the variation changes after the subunit of 6.5b'.

the arrow with (1m0) correspond to the (110) spot shown in Fig. 4. The arrow labeled by (100) indicates the position of $k = 0$. The spacing of superstructure spots becomes narrow gradually with the decrease of WO$_3$ content. The superstructure spots of sample W10A shown in (e) of Fig. 5 are commensurate and can be indexed on the unit cell with 8b'. The other superstructure spots are, however, incommensurate.

3.3. Mean Multiplicity

The spacing of the superstructure spots s^* in the (001) diffraction pattern as shown in Fig. 4 is proportional to the inverse of a mean length of the contrast modulation S in the HREM image as shown in Fig. 1. The mean multiplicity $\bar{m}$ obtained by S/b' in a HREM image must equal b'^*/s^* in a diffraction pattern. The lengths of b'^* and s^* were measured on enlarged photographs of the (001) diffraction pattern films, and then $\bar{m}$ was calculated by $\bar{m} = b'^*/s^*$. For example, the values of $\bar{m}$ obtained from (d) and (f) of Fig. 5 are 7.714 and 8.585. Let us consider the relationship between the mean multiplicity $\bar{m}$ and the multiplicity m.

The diffraction pattern consists of two kinds of clusters of spots parallel to b'^* as shown in Fig. 4. One labeled by upward arrows, named F, includes one fundamental spot of the orthorhombic subcell and four superstructure spots on both sides of the fundamental spot. The other labeled by downward arrows, named H, includes four superstructure spots. The cluster H appears twice between two Fs along the b'^*. The change of an array of (1k0) electron diffraction spots is schematically shown in Fig. 6, based on the present electron diffraction patterns and the crystallographic data of four kinds of compounds previously reported. The full circles and their sizes express positions and intensities of electron diffraction spots. The open circles denote weak spots. The diffraction spots of $\bar{m} = 6.5$, 8, 9.5, and 11, which are mean multiplicities of the compounds of Ta$_{22}$W$_4$O$_{67}$, Ta$_{30}$W$_2$O$_{81}$, Ta$_{38}$WO$_{98}$, and Ta$_2$O$_5$, are commensurate. A distance d^* between adjacent two clusters of spots F and

FIG. 2. An enlarged photograph of Fig. 1. The black dots giving rise to lattice fringes correspond to columns of metal atoms. Full circles represent approximate positions of the metal atoms and the rectangle with a' and b' corresponds an orthorhombic subcell. Lattice fringes have a modulation in their contrast. The contrast modulation has a sequence of 8, 8, 8, 6.5, 8, 8, and 8b', which were determined from a variation of the spacing of the black dots shown in Fig. 3. The mean multiplicity of this crystal fragment is 7.7.
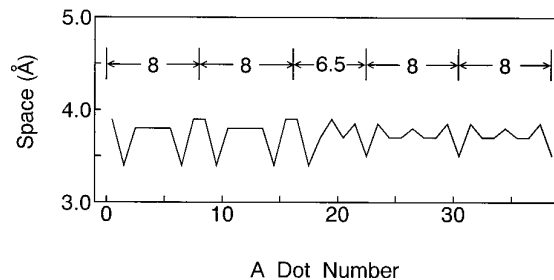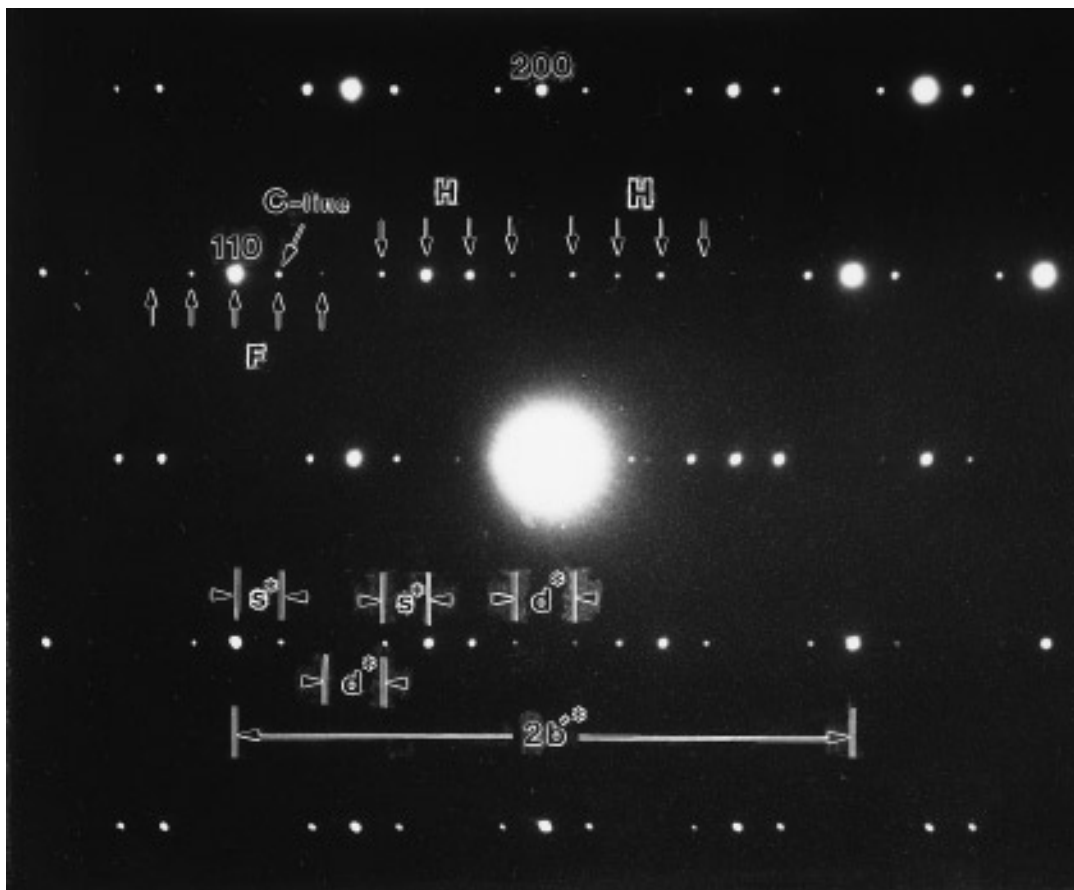
FIG. 4. A (001) electron diffraction pattern of an L-Ta$_2$O$_5$-type crystal of sample W20A. Fundamental spots indexed on an orthorhombic subcell and incommensurate superstructure spots are seen. The diffraction pattern consists of two clusters of spots parallel to b'^*: the cluster, named F, labeled by upward arrows and the cluster, named H, labeled by downward arrows. Distances s^* and d^* denote a spacing of the superstructure spots and a space between adjacent clusters of spots, respectively. The next spot on the right side of the (110) corresponds to a C-line characterized by Moser (21).

H equals one between adjacent two clusters of spots H and H in the present system as shown in Fig. 4. So the b'^* is expressed as $b'^* = 5s^* + 1.5d^*$. For indexing spots, the lengths of s^* and d^* were measured on enlarged photographs of the (001) diffraction pattern films, and then a set of integers (k_s, k_d) has been chosen, where the relation $k_s : k_d = s^* : d^*/2$ has to be satisfied. Hence,

$$b'^* = 5s^* + 1.5d^*$$
$$= 5k_s(d^*/2k_d) + 3k_d(d^*/2k_d).$$

If k_s and k_d does not have a common factor, $d^*/2k_d$ is the longest b^* in superlattices considered. So $d^*/2k_d$ has been adopted as a b^* of the superlattice. Hence,

$$b'^* = (5k_s + 3k_d)b^*$$
$$= mb^*.$$

Therefore, the b'^* has a multiplicity $m = 5k_s + 3k_d$ of the b^*. In real space, the b axis of the superlattice has a multiplicity $m = 5k_s + 3k_d$ of the b' of the subcell. For example, the multiplicities of the diffraction patterns as shown in (d) and (f) of Fig. 5 are expressed as $m = 5 \times 21 + 3 \times 19 = 162$ and $m = 5 \times 41 + 3 \times 49 = 352$. The mean multiplicity is related to the multiplicity as follows:

$$\overline{m} = b'^*/s^*$$
$$= mb^*/s^*$$
$$= m(d^*/2k_d)/(k_sd^*/2k_d)$$
$$= m/k_s.$$

If s^* equals d^*, $d^*/2$, $d^*/3$, $d^*/4$, $d^*/5$, $d^*/6$, ..., m is 13, 8, 19, 11, 25, 14, ... and $\overline{m}$ is 6.5, 8, 9.5, 11, 12.5, 14, ..., that is, the superstructure spots are commensurate as shown in Fig. 6. The commensurate phases in the present system
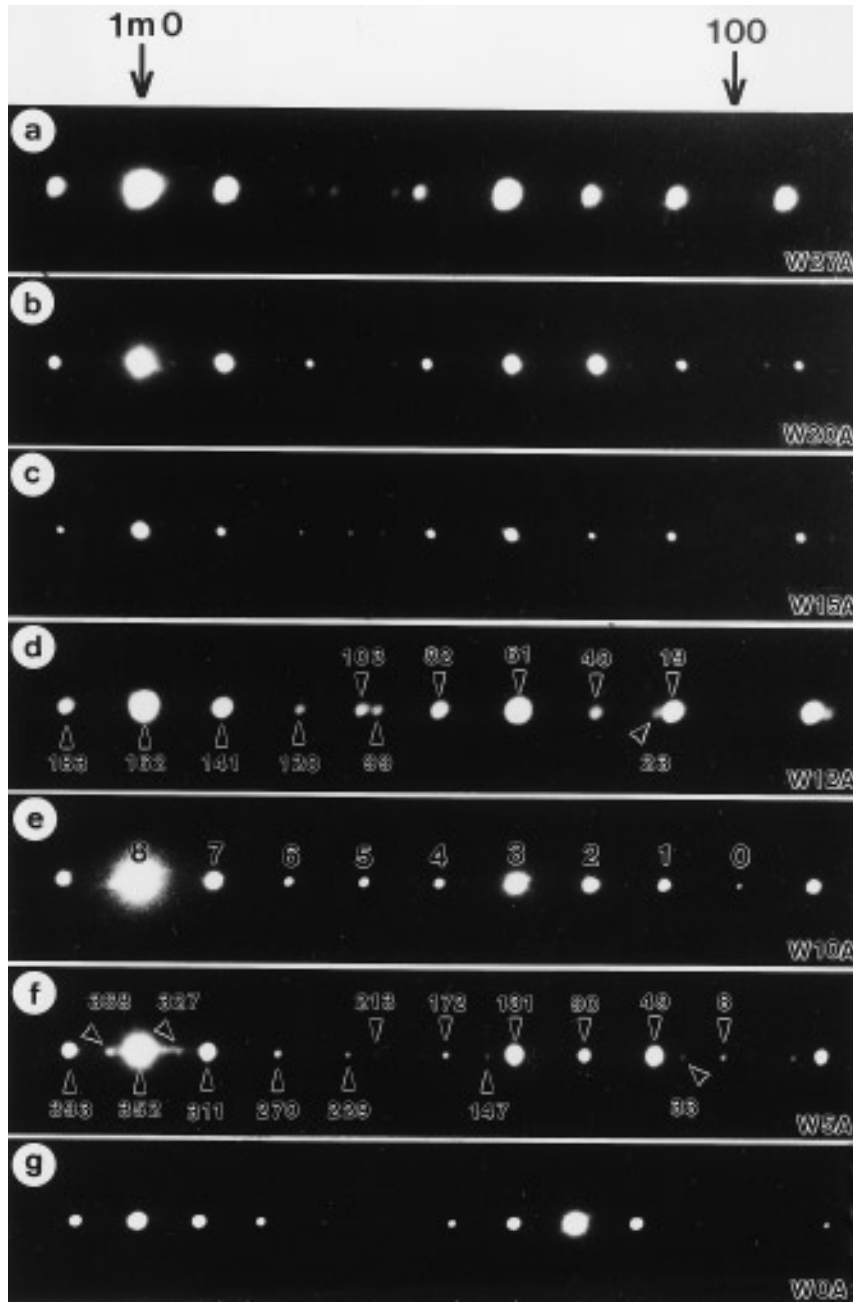
FIG. 5. Arrays of electron diffraction spots ($1k0$) of samples annealed at 1400°C in air; here k denotes an index by a superlattice. The spots indicated by an arrow with ($1m0$) correspond to (110) indexed on an orthorhombic subcell. An arrow labeled by (100) indicates the position of $k = 0$. The spacing of superlattice spots becomes narrow gradually with the decrease of WO₃ content. Figures by spots are indices k determined by a manner described in Section 3.3. See text for details.

are expected to consist of only one subunit. The minimum subunit is 6.5 times b'. The subunit lengthens by $1.5b'$. The multiplicity of an intermediate structure is expressed as $m = pm_i + qm_{i+1}$ by a way of Anderson's description, where m_i and m_{i+1} are multiplicities of subunits 6.5, 8, 9.5, 11, 12.5, 14, ..., and p and q are the number of the two subunits. The mean multiplicity is also defined as $\bar{m} =$

$m/(p + q)$. Therefore, k_s denotes the number $(p + q)$ of subunits in the superlattice with infinitely adaptive structures. The values of $\bar{m}$ and k_s characterize the superstructures. If a value of $\bar{m}$ is between 6.5 and 8, the superstructure consists of the subunits with $6.5b'$ and $8b'$. For example, the structures of crystals showing the diffraction patterns of $\bar{m} = 7.714$ and $k_s = 21$ (d), $\bar{m} = 8.585$ and $k_s =$
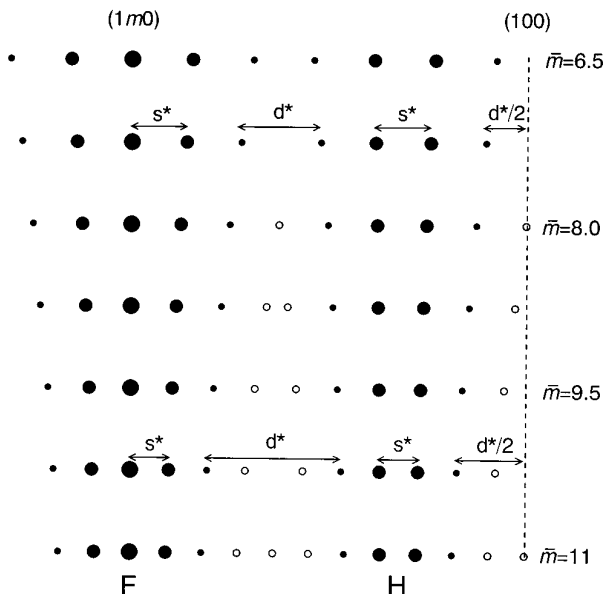
FIG. 6. A schematic representation of arrays of $(1k0)$ electron diffraction spots of superstructures with $\overline{m} = 6.5–11$. Full circles and their size express positions and intensities of spots. Open circles denote weak spots. Distances s^* and d^* correspond to those in Fig. 4. The clusters of spots named F and H, which contain five and four spots, represent spots labeled by upward and downward arrows in Fig. 4.
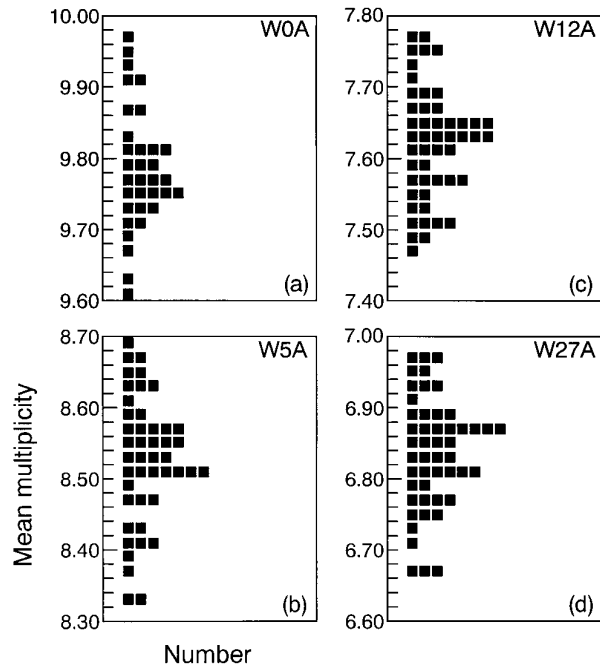

FIG. 7. Histograms of mean multiplicities obtained from b'^*/s^* in (001) electron diffraction patterns of samples W0A(a), W5A(b), W12A(c), and W27A(d). A distribution in each histogram looks like a Gaussian, which results from a distribution of infinitely adaptive structures in samples.
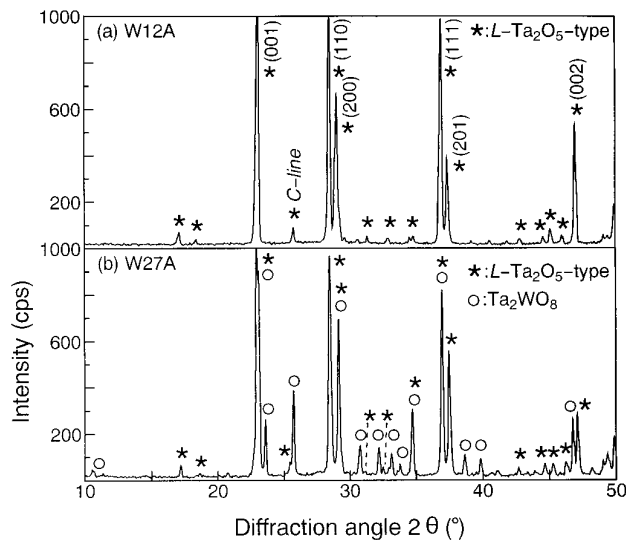
41 (f) in Fig. 5 are expressed as $m = 4 \times 6.5 + 17 \times 8 = 162$ and $m = 25 \times 8 + 16 \times 9.5 = 352$, respectively. Thus, $\overline{m}$ is convenient for the interpretation of infinitely adaptive structures in the present system. The histograms of $\overline{m}$ about 50 crystal fragments in the present samples exhibit a nearly Gaussian distribution as shown in Fig. 7.

3.4. X-Ray Diffraction

An X-ray diffraction diagram of the sample composed of L-Ta_2O_5-type compounds only has strong diffraction peaks indexed by the orthorhombic subcell and numerous weak peaks of the superstructure as shown in (a) of Fig. 8. A sample in the two phase region with an L-Ta_2O_5-type compound and Ta_2WO_8 (22) gives an X-ray diffraction pattern as shown in (b) of Fig. 8. The peaks labeled by asterisks and open circles correspond to reflections from L-Ta_2O_5-type crystals and Ta_2WO_8 crystals, respectively. The diffraction peak about $25°2\theta$ is a C-line. The mean multiplicity $\overline{m}$ is calculated by the following equation based on a geometrical relationship of the (001) diffraction plane:

$$\overline{m} = \frac{\sqrt{\sin^2 \theta - (1/4) \sin^2 \theta_a}}{\sqrt{\sin^2 \theta - (1/4) \sin^2 \theta_a} - \sqrt{\sin^2 \theta_c - (1/4) \sin^2 \theta_a}}.$$

Here θ, θ_a, and θ_c are diffraction angles of the (110) reflection, the (200) reflection, and the C-line reflection in the

FIG. 8. Powder X-ray diffraction diagrams of samples W12A(a) and W27A(b). Peaks labeled by asterisks are diffracted from L-Ta_2O_5-type crystals and peaks labeled by open circles are diffracted from Ta_2WO_8 crystals. The strong diffraction peaks of the L-Ta_2O_5-type structure are indexed on an orthorhombic subcell. The peak about $25°2\theta$ is a C-line characterized by Moser (21).

TABLE 2
Mean Multiplicities of Samples Quenched

Sample name	$\overline{m}$ from electron microscopy		X-ray diffraction analysis			
	EDP	HREM image	$\overline{m}$	2θ (°)	$2\theta_a$ (°)	$2\theta_c$ (°)
W0A	9.767 ± 0.146	9.75–9.87	9.726	28.450	28.973	26.274
W5A	8.534 ± 0.119	8.56–8.64	8.522	28.487	29.059	26.010
W10A	7.984 ± 0.083	7.82–7.96	7.819	28.482	29.074	25.789
W12A	7.625 ± 0.082	7.57–7.68	7.573	28.503	29.058	25.720
W15A	7.402 ± 0.070	7.33–7.49	7.332	28.400	29.083	25.548
W20A	6.994 ± 0.084	6.96–7.15	7.058	28.310	28.954	25.357
W27A	6.841 ± 0.083	6.80–6.93	6.888	28.509	29.187	25.465

X-ray diffraction pattern. The results are listed in Table 2 with the results of the electron diffraction and the HREM observation.

3.5. Simulation of Electron Diffraction Pattern

Kinematical electron diffraction patterns have been calculated based on the infinitely adaptive structure model. The data obtained by tracing the black dots in the HREM images were used as position data of metal atoms of the subunits with $6.5b'$ and $8b'$. The positions of oxygen atoms were determined taking account of Stephenson and Roth's results (2–5) so that the oxygen atoms were polyhedrally arranged around the metal atoms. In general, the scattering amplitude G from a whole crystal is represented by

$$G(\mathbf{r}^*) = \sum_{\text{crystal}} f_j(\mathbf{r}^*) \exp(2\pi i \mathbf{r}_j \mathbf{r}^*),$$

where f_j is an atomic scattering factor for electron of the jth atom, $\mathbf{r}^*$ a vector in reciprocal space, and $\mathbf{r}_j$ a position vector of the jth atom in real space. In the case of an infinitely adaptive structure, a crystal consists of l subunits and the gth subunit has a multiplicity m_g of the subcell with n atoms, and G is transformed to the following equation:

$$G(\mathbf{r}^*) = \sum_{g=1}^{l} \sum_{h=1}^{m_g} \sum_{j=1}^{n} f_j(\mathbf{r}^*) \exp 2\pi i \left[\mathbf{u}_j + \Delta\mathbf{u}_{jhg} \right.$$
$$\left. + \left\{ \left(\sum_{g'=1}^{g-1} m_{g'} \right) + h - 1 \right\} \mathbf{b}' \right] \mathbf{r}^*.$$

Then, the amplitude of a $(1k0)$ reflection is given by

$$G(k) = \sum_{g=1}^{l} \sum_{h=1}^{m_g} \sum_{j=1}^{n} f_j(k) \exp 2\pi i \left[x_j + \Delta x_{jhg} \right.$$
$$\left. + \left\{ y_j + \Delta y_{jhg} + \left(\sum_{g'=1}^{g-1} m_{g'} \right) + h - 1 \right\} k \right].$$

Here $\mathbf{u}_j$, x_j, and y_j are a position vector and position parameters of the jth atom in each subcell, $\Delta\mathbf{u}_{jhg}$, Δx_{jhg}, and Δy_{jhg} denotes shifts of the jth atom of the hth subcell in the gth subunit, which correspond to a structure modulation mentioned in Section 3.1. The index k is based upon the orthorhombic subcell. The intensity of the diffraction pattern is given by

$$I(k) = G(k) \cdot G^*(k),$$

where G^* is the complex conjugate of the amplitude.

Results of the calculation on the infinitely adaptive structure model with $\overline{m} = 7$ are shown in Fig. 9. Two models consisting of 146 units of $6.5b'$ and 73 units of $8b'$ were prepared. One has an ordered structure with a sequence of 6.5, 6.5, and $8b'$. The other has six irregularities, as three excesses and three deficiencies of a $6.5b'$ randomly happen in the sequence. Their structures are expressed as $73 \times (2 \times 6.5 + 1 \times 8)$ for the ordered model and $67 \times (2 \times 6.5 + 1 \times 8) + 3 \times (3 \times 6.5 + 1 \times 8) + 3 \times (1 \times 6.5 +$
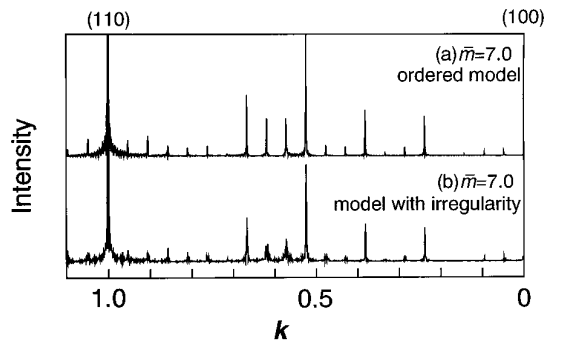

FIG. 9. Profiles of calculated intensities of $(1k0)$ reflections on two models with a mean multiplicity of 7; here k denotes an index on an orthorhombic subcell. One is an ordered model with a sequence of 6.5, 6.5, and $8b'$ (a). The other has six irregularities as an excess and a deficiency of $6.5b'$ in the sequence (b). Peak positions of two profiles are the same. See text for details.
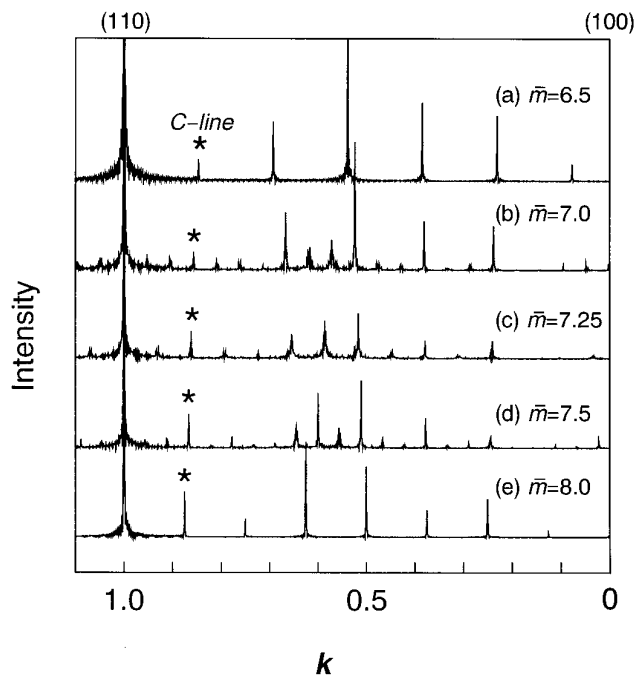
FIG. 10. Profiles of calculated intensities of $(1k0)$ reflections on models with mean multiplicities of 6.5 (a), 7 (b), 7.25 (c), 7.5 (d), and 8 (e); here k denotes an index on an orthorhombic subcell. The peak positions of superstructure reflections, for example, a C-line, continuously shift with the mean multiplicity. The peaks with $k = 0.1–0.7$ and $k = 0.7–1.1$ belong to the clusters of spots H and F, respectively. See text for details.

with $k = 0.1–0.7$ and $k = 0.7–1.1$ belong to the clusters of the diffraction spots named H and F, respectively.

3.6. Phase Analysis

The mean multiplicities obtained from the electron diffraction in each sample are listed in Table 3 with the results of phase analyses by X-ray. The mean multiplicity continuously varies with WO_3 content. It also depends on annealing temperatures as shown in Fig. 11. The samples annealed at 700°C after calcination at 1400°C have the same mean multiplicities and the same standard deviations as those

1×8) for the model with irregularity. The irregular model cannot be prepared by Anderson's description, because his model requires a continuance of an even number of 6.5. There is no difference in positions of the calculated diffraction peaks between the ordered model and the model with irregularity shown in (a) and (b) of Fig. 9. The calculated peaks of the model with irregularity are somewhat wider than those of the ordered model. The difference, however, is too slight to be distinguished experimentally. The profile of the diffraction intensity varies with the superstructure. The diffraction intensities of the models with $\overline{m} = 6.5$, 7.25, 7.5, and 8 were also calculated. Their structures are expressed as $210 \times (1 \times 6.5)$ for $\overline{m} = 6.5$, $99 \times (1 \times 6.5 + 1 \times 8) + 3 \times (1 \times 6.5 + 2 \times 8) + 3 \times (1 \times 8)$ for $\overline{m} = 7.25$, $66 \times (1 \times 6.5 + 2 \times 8) + 2 \times (1 \times 6.5 + 3 \times 8) + 2 \times (1 \times 6.5 + 1 \times 8)$ for $\overline{m} = 7.5$, and $210 \times (1 \times 8)$ for $\overline{m} = 8$. Six and four irregularities of the sequence randomly exist in the models with $\overline{m} = 7.25$ and 7.5. The models have a long b axis of about 6000 Å so that Laue's interference function scarcely has an influence on the calculated profiles of the $(1k0)$ reflections shown in Fig. 10. The peak positions of superstructure reflections continuously shift with the mean multiplicity. The peaks

TABLE 3
Results of the Present Study

Composition Ta$_2$O$_5$: WO$_3$ WO$_3$ mol%	Sample name	Phase[a] analysis by X-ray	$\overline{m}$ from EDP	Specimen's color
1:0	W0A	L	9.767	cream
0	W0B	L	9.816	light cream
	W0C	L	10.029	white
	W0C′	L	10.162	white
	W0D	L	9.816	white
	W0E	L	11.883	white
	W0F	L	12.461	white
	W0F′	L	12.653	white
	W0G	L	12.484	white
37:2	W5A	L	8.534	cream
5.1	W5B	L	8.491	light cream
	W5B′	L	8.486	pale yellowish ocher
	W5C	L	9.002	white
	W5D	L	8.447	white
	W5E	L	9.082	white
	W5F	L	9.449	white
	W5F′	L	9.253	white
	W5G	L	9.194	white
9:1	W10A	L	7.984	cream
10	W10B	L	7.974	light cream
	W10B′	L	7.988	pale yellowish ocher
	W10C	L	8.090	white
	W10D	L	7.989	white
	W10E	L	8.089	white
15:2	W12A	L	7.625	cream
11.8	W12F	L	7.937	white
	W12F′	L	8.030	white
	W12G	L	8.010	white
17:3	W15A	L	7.402	cream
15	W15B	L	7.416	light cream
	W15B′	L	7.518	pale yellowish ocher
	W15C	L	7.507	white
	W15D	L	7.404	white
	W15E	L	7.653	white
4:1	W20A	L	6.994	cream
20	W20B	L	7.030	light cream
	W20B′	L	7.040	light grayish brown
	W20C	L	7.102	white
	W20D	L	6.930	white
	W20E	L	7.099	white

TABLE 3—*Continued*

Composition Ta$_2$O$_5$:WO$_3$ WO$_3$ mol%	Sample name	Phase[a] analysis by X-ray	$\overline{m}$ from EDP	Specimen's color
79:21	W21B	L	6.912	light yellowish white
21	W21G	L	7.063	white
39:11	W22B	L + TW	6.904	light yellowish white
22	W22G	L	7.093	white
77:23	W23B	L + TW	6.824	light yellowish white
23	W23G	L + TW	7.030	white
38:12	W24B	L + TW	6.800	light yellowish white
24	W24G	L + TW	7.052	white
3:1	W25B	L + TW	6.868	light yellowish white
25	W25G	L + TW	7.056	white
11:4	W27A	L + TW	6.841	light yellowish white
26.7	W27F	L + TW	7.321	white
	W27F'	L + TW	7.126	white
	W27G	L + TW	7.006	white
7:3	W30B	L + TW	6.893	yellowish white
30	W30G	L + TW	7.217	white
13:7	W35B	TW	—	yellowish white
35	W35G	TW	—	white
3:2	W40B	TW	—	yellowish white
40	W40G	TW	—	white

[a] L means *L*-Ta$_2$O$_5$-type phases and TW means Ta$_2$WO$_8$.

FIG. 12. The effect of annealing temperatures on mean multiplicities plotted versus WO$_3$ content. The effect is apparent at less than 10 mol% of WO$_3$ content. The samples cooled at 1000°C have the same mean multiplicities as those cooled to 100°C. A lower end of the mean multiplicity is about 7. A heat treatment in Ar gives the same mean multiplicities as that in air.
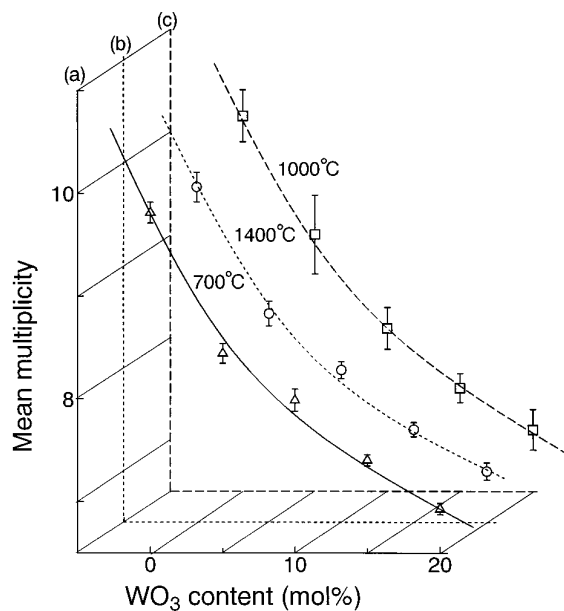

FIG. 11. Mean multiplicities plotted versus WO$_3$ content. A dotted line shows a relation on samples annealed at 1400°C in air (b). Reannealing at 700°C on the samples scarcely changes the relation as shown by a solid line (a). However, the mean multiplicities and their standard deviations become large and wide after reannealing at 1000°C as shown by a broken line (c).
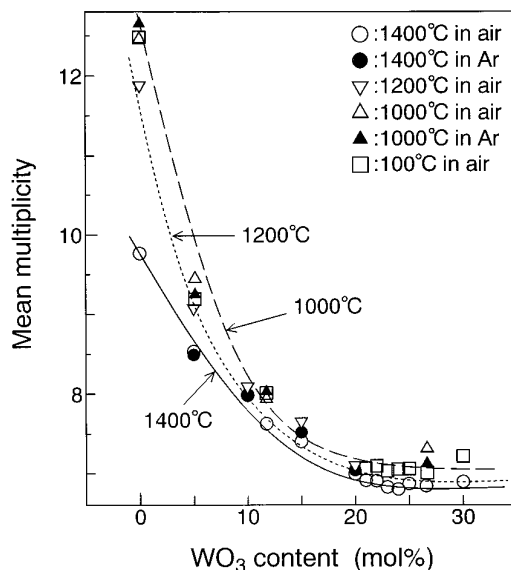
quenched from 1400°C. The other hand, the samples annealed at 1000°C after calcination at 1400°C have larger values and wider standard deviations of the mean multiplicities. Therefore, the mean multiplicities in equilibrium at 1000°C are larger than those at 1400°C and it is possible for samples to change the structure at 1000°C. If the cooling rate is very slow, structures in equilibrium are considered to be complete at any temperatures. Figure 12 shows the results of the samples annealed at 1000°C and 1200°C after cooling by 1.43°C per hour from 1400°C.

The mean multiplicities become large with the decrease of temperature. The effect of temperature is apparent at less than 10 mol% of WO$_3$ content. The structural change will not occur at temperatures below 1000°C, because the samples cooled to 1000°C have the same mean multiplicities as those cooled to 100°C. The lower end of a mean multiplicity in the present study is considered to be about 7.0 at more than about 22 mol% of WO$_3$ content. The Ta$_2$WO$_8$ crystals appeared at more than 22 mol% of WO$_3$ content and the *L*-Ta$_2$O$_5$-type structure disappeared at more than 30 mol% of WO$_3$ content. So the two phase region may extend to 22 mol% of WO$_3$ content at temperatures below 1400°C. Therefore, I have proposed iso-mean-multiplicity lines as shown in Fig. 13. Dotted lines and figures by them denote expected mean multiplicities from the present experiments. Solid lines show the modified phase diagram after the reports of Roth *et al.* (1) and Roth (23).
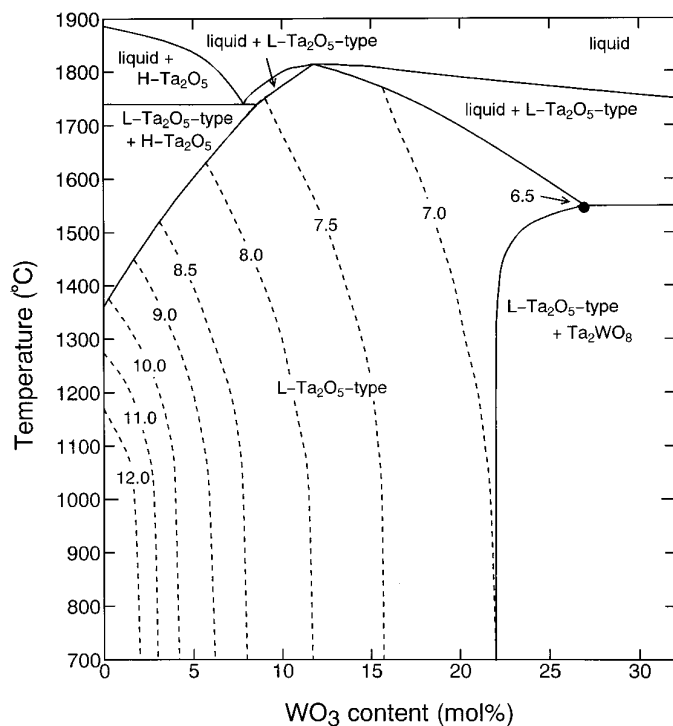
FIG. 13. A proposed phase diagram by the present experiment. Dotted lines and figures by them denote iso-mean-multiplicity lines and their mean multiplicities. With the decrease of temperature, a lower end of the mean multiplicity becomes large and two phase region of an L-Ta_2O_5-type structure and Ta_2WO_8 expands to a lower WO_3 content. Solid lines show the modified phase diagram after the report by Roth *et al.* (1) and Roth (23).

3.7. Sample Color and TGA

A color of the sample depends on heat treatment as shown in Table 3. Annealing at 1400°C made samples with a small WO_3 content light cream. The color of samples became light yellowish white with the increase in WO_3 content. The samples changed from light cream to white by annealing at 1000°C. The sample's color was white at 1200°C and below. Annealing at 1400°C in Ar made a specimen pale ocher. The samples annealed at 1000°C in Ar held white. The heat treatment in Ar, however, gave the same mean multiplicities as the heat treatment in air. The samples heated at 1400°C in Ar were annealed again at 1000°C in the TGA unit with oxygen gas flowing. The samples turned white, however, an increase of weight was not detected. The change of weight is considered to be less than 0.1%.

4. DISCUSSION

Every (001) electron diffraction pattern can be accurately indexed by the manner described in Section 3.3. The multiplicity determined by this manner, however, often

becomes very large. If the clusters of the diffraction spots named F are commensurate with the clusters of the diffraction spots named H as $\overline{m} = 6.5, 8, 9.5, 11, 12.5, 14, \ldots$, the crystal is composed of only one kind of the subunit. Such subunits will appear as a periodic contrast pattern in an electron microscopic image under the condition that superstructure spots are excited. The contrast modulation with a bright band and a dark band as shown in Fig. 1 can be interpreted as a contrast reflecting a subunit. The lattice images corresponding to subunits of 6.5, 8, 9.5, 11, and 14 have been reported (18, 24, 25). On the HREM image, the contrast is generated by a shift and growth of a black dot as mentioned in Section 3.1. If black dots are arranged with a regular space, such a contrast modulation does not appear. The contrast decreases in the area at the crystal edge because of a black dot being small. The contrast increases in the inside of the crystal, because a black dot grows large with a crystal thickness. Black dots touch at narrow spaces, so that dark bands appear and white dots are noticeable at wide spaces in dark bands.

The theory of an approximation of a weak-phase object explains that black dots in a HREM image of a thin crystal reflect positions of metal atoms, so the black dots in Fig. 1 and Fig. 2 are considered to represent approximate positions of metal atoms. The HREM image confirmed the existence of the subunits of $6.5b'$ and $8b'$. So even the subunit of $6.5b'$ should be regarded as a component of the superstructures, because an isolated subunit of $6.5b'$ exists in the matrix of subunit $8b'$ as shown in Fig. 2. The variation of spacing of the black dots shown in Fig. 3 will mirror the variation of the positions of metal atoms. Furthermore, the subunit proposed in the present paper grows large every $1.5b'$. The variation of spacing of the black dots suggests an existence of a structure modulation, which corresponds to the modulation wave vector proposed by Schmid *et al.* (10). Rae *et al.* have shown displacements of metal atoms as a modulation function. The form of their modulation wave is different from my result as shown in Fig. 3. Their concept is, however, in accordance with mine on the existence of the modulation wave. Image simulations on the present structure models by the multi-slice method showed such a contrast variation. A black dot grows large with the increase in crystal thickness and the positions of the black dots scarcely shift until a crystal thickness of about 100 Å. A black dot reflects a position of a metal column along the c axis under an optimum defocus condition until a crystal thickness of about 100 Å. Details will be reported in a near future.

The great interest in this system is whether a structural period corresponding to every space of superstructure spots continuously varying exits or not. I think it does not, because a structural period is essentially discrete. Therefore, an intermediate structure between two commensurate phases should be expressed as $m = pm_i + qm_{i+1}$.

The multiplicity m_i of subunits is 5, 8, 11, and 14 in Roth and Stephenson's description, which cannot explain an isolated subunit of $6.5b'$. Williams et al.'s m_i is 13, 16, 19, 22, 25, 28, 31, and 34, which is multiplicity of $b'/2$ and twice mine. If only one sequence of subunits is available for a multiplicity, the system is interpreted to be a continuum of an infinite number of line phases. The shift-lattice model by Williams et al. has a unique sequence for a multiplicity, so they regarded this system as an ordered intergrowth structure. I think, however, every sequence of subunits is potentially available for a set of p and q. The structures are polymorphs of each other and the polymorphism will be able to coexist. It is reasonable that a structure with subunits distributed fairly evenly is a thermodynamically stable phase. Therefore, infinitely adaptive structures in this system are described as a solid solution at a subunit level between adjacent two subunits. The mean multiplicity expresses a feature of the superstructure with a solid solution better. Schmid et al. refined the structures of two commensurate phases and found a modulation wave in their structures. They described that the present system has been interpreted as a solid solution model with an incommensurately modulated structure, but they did not concretely explain structures of intermediate phases.

The present description in Section 3.3, the shift-lattice by Williams et al., and the primary modulation wave vector by Schmid et al. are only geometric interpretations about the reciprocal lattice on the (001) diffraction pattern. These interpretations cannot give information about a sequence of subunits of an incommensurate phase. A HREM observation can be made in the thinner area of the crystal edge which satisfies an approximation of a weak-phase object. The HREM image in Fig. 2 shows a sequence of subunits. The sequence was determined by marking a bright band and a dark band. The black dots close and the white dots grow large in the dark bands. The space between the black dots varies periodically. This is different from the shift-lattice model. Therefore, observed structures are not interpreted as an ordered intergrowth structure as proposed by Harburn et al. (14). As mentioned in a previous paper (18), the subunit of $6.5b'$ does not have orthorhombic symmetry. Figure 2 shows that the b' axis of the subcell shifts by $a'/2$ at the boundary between the subunits of $6.5b'$ and $8b'$. The b' axis will return to previous direction after the second subunit of $6.5b'$. If the superstructure has an even subunit of $6.5b'$, it holds orthorhombic symmetry. The mean multiplicity $\overline{m}$ of the crystal fragment shown in Fig. 2 is 7.7. The structure is expressed as $2 \times 6.5 + 8 \times 8$ in the present description and $1 \times 5 + 9 \times 8$ in Anderson's. The sequence is expected to be ... [6.5, 8, 8, 8, 8, 6.5, 8, 8, 8, 8] ... in the present description and ... [5, 8, 8, 8, 8, 8, 8, 8, 8] ... in Anderson's. An isolated subunit of $5b'$ should exist in a matrix of the subunit of $8b'$, if Anderson's

description is correct. A subunit of $5b'$ has never been observed in HREM images.

The distribution of the mean multiplicity as shown in Fig. 7 will result from not only experimental errors but also a distribution itself of infinitely adaptive structures in samples because of equilibrium not being completely achieved. So a standard deviation of the mean multiplicity denotes a degree of the achievement of equilibrium. The samples are, however, single phases on X-ray diffraction. The values of $\overline{m}$ obtained by X-ray diffraction accord with those by HREM image and electron diffraction as shown in Table 2. This fact suggests that each sample is generally homogeneous and the average value of $\overline{m}$ obtained by electron diffraction is a mean multiplicity of a completely homogeneous sample. The obtained mean multiplicities in the present paper were somewhat smaller than the results of Stephenson and Roth's and Williams et al.'s, which were modified into our mean multiplicity. The difference is considered to result from the preparation of samples. In the present experiments, mean multiplicities plotted versus WO$_3$ content fit on curves well as shown in Figs. 11 and 12. So obtained mean multiplicities are reliable. The minimum and maximum values of $\overline{m}$ are about 6.8 and 12.7. The structures are expressed as $4 \times 6.5 + 1 \times 8$ and $14 \times 12.5 + 2 \times 14$. Therefore, possible subunits are 6.5, 8, 9.5, 11, 12.5, and 14 in the present investigation.

The results of the simulation of the electron diffraction pattern have shown a good agreement with a feature of the experimental $(1k0)$ electron diffraction pattern. The spacing of the superlattice spots s^* and the distance d^* between the clusters of spots continuously vary with the mean multiplicity. The weak diffraction peaks appear around 0.6 of k and on the left side of C-lines in (b), (c), and (d) of Fig. 10. These peaks correspond to the spots labeled by 99 and 103 in (d) and 213, 229, and 327 in (f) of Fig. 5. The calculated diffraction peaks of the ordered model have a higher intensity than those of the model with irregularity. If the irregularity occurs in the sequence of subunits as described in Section 3.5; this is interpreted as a stacking fault, the reflection peaks becoming somewhat lower and wider. In general, stacking faults are expected to cause a streaking in a diffraction pattern, but no streaking appears in the calculated profiles in (b), (c), and (d) of Fig. 10, which are diffraction patterns of the models with four or six irregularities. The HREM observations found irregularities in sequences of subunits (18). There was, however, no streaking in the (001) diffraction pattern as shown in Fig. 4. This is important for the interpretation of the present infinitely adaptive structures. The irregularity should be interpreted as a solid solution at a subunit level. The modulation of the position of metal atoms travels periodically over the crystal lattice and the subunits form. The irregularity in the sequence of subunits will scarcely give an influence on the modulation of the positions of

metal atoms, so that the electron diffraction pattern has no streaking along the $b*$ axis.

The $Ta_{22}W_4O_{67}$ crystal with a mean multiplicity of 6.5, which had been reported as the end of the infinitely adaptive structures with the richest WO_3 content of 26.7 mol% (2), has not appeared in the present experiment. As I have proposed in Fig. 13, the two phase region of an L-Ta_2O_5-type structure and Ta_2WO_8 extends with the decrease of temperature. It reaches down to 22 mol% of WO_3 content at temperatures below 1400°C. A sample with a high WO_3 content will have a mean multiplicity of 6.5, if it is annealed at 1550°C. At low WO_3 contents the structure sensitively depends upon temperature and WO_3 content. So the space of the iso-mean-multiplicity lines are narrow at a low WO_3 content and the lines bend at high temperature. In addition, I have not observed H-Ta_2O_5 crystal at 1400°C. The high-temperature phase will quickly transform into the low-temperature phase even by rapid quenching.

In the present system, the quenching is effective in holding an L-Ta_2O_5-type structure. The reason is considered as follows: there is a little difference among L-Ta_2O_5-type structures, the profit of a free energy obtained by the structural change is small for an activation energy of the structural change, and low temperatures seldom give an activation energy of the structural change. The structural change occurs at more than 1000°C and goes very slowly so that the samples annealed at 1000°C have a wider standard deviation than those annealed at 1400°C as shown in Fig. 11.

The color of the samples annealed at 1400°C is considered to result from the deficiency of oxygen. There is no difference in the mean multiplicity between the heat treatment in air and Ar as shown in Fig. 12. Reannealing at 700°C made the samples heated at 1400°C white, but the mean multiplicities of them scarcely changed as shown in Fig. 11. The samples are reduced at 1400°C, and they absorb oxygen in air below 1200°C. They also absorb oxygen included as an impurity in Ar below 1200°C, so they become white. The reduction and absorption of oxygen is so little that TGA cannot detect it. If the reduction generates a distortion plane as proposed by Stephenson and Roth (7), the mean multiplicity increases with the distortion plane. In the present experiment, however, the mean multiplicity decreased at high temperature. The change of color may occur only on the surface of a crystal and the reduction may not progress into a crystal. Therefore, the mean multiplicity depends upon only temperature at each composition in the present experiment. The difference of the mean multiplicity by temperature is also interpreted as polymorphism as the pure L-Ta_2O_5.

REFERENCES

1. R. S. Roth, J. L. Waring, and H. S. Parker, *J. Solid State Chem.* **2,** 445 (1970).
2. N. C. Stephenson and R. S. Roth, *Acta Crystallogr. B* **27,** 1010 (1971).
3. N. C. Stephenson and R. S. Roth, *Acta Crystallogr. B* **27,** 1018 (1971).
4. N. C. Stephenson and R. S. Roth, *Acta Crystallogr. B* **27,** 1031 (1971).
5. N. C. Stephenson and R. S. Roth, *Acta Crystallogr. B* **27,** 1037 (1971).
6. K. Lehovec, *J. Less-Common Met.* **7,** 397 (1964).
7. R. S. Roth and N. C. Stephenson, "Chemistry of Extended Defects in Non-Metallic Solids," (L. Eyring and M. O'Keefe, Eds.), p. 167. North-Holland, Holland, Amsterdam, 1970.
8. J. S. Anderson, *J. Chem. Soc. Dalton Trans.,* 1107 (1973).
9. K. Kosuge, "Chemistry of Non-Stoichiometric Compounds," p. 189. Oxford Univ. Press, Oxford, 1994.
10. S. Schmid, R. L. Withers, and J. G. Thompson, *J. Solid State Chem.* **99,** 226 (1992).
11. S. Schmid, J. G. Thompson, A. D. Rae, B. D. Butler, R. L. Withers, N. Ishizawa, and S. Kishimoto, *Acta Crystallogr. B* **51,** 698 (1995).
12. A. D. Rae, S. Schmid, J. G. Thompson, R. L. Withers, and N. Ishizawa, *Acta Crystallogr. B* **51,** 709 (1995).
13. J. M. Williams, R. J. D. Tilley, G. Harburn, and R. P. Williams, *J. Solid State Chem.* **92,** 460 (1991).
14. G. Harburn, R. J. D. Tilley, J. M. Williams, R. P. Williams, and J. Hutchison, *J. Chem. Soc. Faraday Trans.* **88,** 621 (1992).
15. G. Harburn, R. J. D. Tilley and R. P. Williams, *Phil. Mag. A* **68,** 633 (1993).
16. J. M. Williams, R. J. D. Tilley, G. Harburn, and R. P. Williams, *J. Chem. Soc. Faraday Trans.* **88,** 325 (1992).
17. G. Harburn, R. J. D. Tilley, J. M. Williams, and R. P. Williams, *Proc. R. Soc. London A* **440,** 23 (1993).
18. T. Miyano and K. Kosuge, *Eur. J. Solid State Inorg. Chem.* **31,** 867 (1994).
19. P. J. England and R. J. D. Tilley, *Chem. Scripta* **24,** 130 (1984).
20. R. Papiernik, B. Gaudreau, and B. Frit, *J. Solid State Chem.* **25,** 143 (1978).
21. R. Moser, *Schweiz. Mineral. Petrogr. Mitt.* **45,** 35 (1965).
22. L. M. Kovba and V. K. Trunov, *Z. Struk. Khimii* **6,** 244 (1965).
23. R. S. Roth, *Prog. Solid State Chem.* **13,** 159 (1980).
24. S. Iijima and J. M. Cowley, *J. Phys. Coll. C7, Suppl. 12* **38,** 135 (1977).
25. T. R. Wagner, *J. Solid State Chem.* **91,** 189 (1991).